

**Role of broadband-laser-pulse temporal extent in  $H_2^+$  photodissociation**E. P. Benis,<sup>1</sup> M. Bakarezos,<sup>2</sup> N. A. Papadogiannis,<sup>2</sup> M. Tatarakis,<sup>2</sup> S. Divanis,<sup>1</sup> C. Ó Broin,<sup>3</sup> and L. A. A. Nikolopoulos<sup>3</sup><sup>1</sup>*Department of Physics, University of Ioannina, GR-45110 Ioannina, Greece*<sup>2</sup>*Centre for Plasma Physics and Lasers, TEI of Crete (CPPL/TEI) Evangelou Daskalaki Street 1, 74100 Rethymno and Romanou Street 3, 73133 Chania, Crete, Greece*<sup>3</sup>*School of Physical Sciences and National Center for Plasma Science and Technology, Dublin City University, Dublin 9, Ireland*

(Received 14 July 2012; published 24 October 2012)

Molecular hydrogen ion ( $H_2^+$ ) dissociation paths of bond softening (BS) and above threshold dissociation (ATD) are investigated exploiting few-cycle chirped laser pulses. 7-fs laser pulses are temporally broadened in a controlled way by the imposed positive chirp covering the range 7–55 fs. The dissociation of the  $H_2^+$  molecules via the BS and ATD paths is then systematically monitored as a function of the pulses duration in conditions of equal  $H_2^+$  yield. The experimental data show distinctive characteristics both in the energy dissociation spectral structure as well as in the yield as the pulse duration broadens. The interpretation of our experimental findings is supported by *ab initio* calculations based on the  $H_2^+$  dissociation time-dependent Schrödinger equation (TDSE) in a strong laser field, thus shedding light into the details of the underlying dissociation dynamics involving few-cycle pulses. The results are also analyzed within the Floquet picture discussing certain limits of its applicability. Finally, our experimental findings show strong molecular alignment for durations longer than 20 fs.

DOI: [10.1103/PhysRevA.86.043428](https://doi.org/10.1103/PhysRevA.86.043428)

PACS number(s): 33.20.Xx, 33.80.Wz, 42.50.Hz

**I. INTRODUCTION**

The behavior of  $H_2$  and  $H_2^+$  in the presence of laser fields has been extensively studied the past twenty years and was boosted by the advent of strong and short duration (fs) lasers (see, e.g., Ref. [1] and references therein). The studies of the benchmark molecules  $H_2$ , HD, and  $D_2$  brought to light a family of new fundamental molecular dissociation mechanisms named in the literature as bond softening (BS) [2], bond hardening [3], above threshold dissociation (ATD) [4], charge resonance enhanced ionization (EI) [5,6], and rescattering [7,8]. A variety of techniques have been developed in order to both study in detail the dissociation mechanisms but also in an attempt to control them suitably. Thus, methods and detection schemes based on typical pump-probe approaches [9–11], the control of the carrier envelope phase (CEP) of the laser pulse [12–14], the exploitation of the pulse duration [3,15–19] and pulse wavelength [4,20,21], as well as the use of two-color fields have been reported in the literature [22–25].

Amongst the above approaches we will focus on the temporal manipulation of the laser pulse via an imposed chirp in order to study the BS and ATD dissociation paths of  $H_2^+$ , a technique that has already been demonstrated in the past [3]. A chirp imposed on the laser pulse, resulting in the pulse's temporal extent, has been shown to control dissociation paths in cases where the duration of the pulse is much longer than the characteristic time of the dynamic process [26]. In such cases, the process may be completed well before the peak of the pulse and the sign of the chirp will obviously play a non-negligible role. Thus, noticeably different dissociation spectra for 45- and 125-fs pulses have been reported in [27]. However, in the cases where the pulse duration, after broadening via the imposed chirp, is smaller or at least of the order of the time scale of the process under study, chirp is not expected to play a major role in the dynamics as long as the bandwidth color spreading is concerned. Then, chirp may well be used as a versatile tool to accurately control the duration of the laser pulse promoting studies of dynamic processes as a function of the pulse duration for pulses having identical bandwidths.

In this work, we attempt a systematic investigation of the  $H_2^+$  dissociation mechanisms of BS and ATD as a function of the duration of the laser pulses, having the same frequency content. The duration of the pulses is varied between 7 and 55 fs in fine steps of  $\leq 8$  fs controlled by an imposed positive chirp and is accurately measured during the experimental process. For consistency reasons, we perform these measurements at constant  $H_2^+$  yield, corresponding to laser peak intensities in the range  $0.2\text{--}1.0 \times 10^{14}$  W/cm<sup>2</sup>. Our findings show distinctive characteristics for increasing pulse durations both in the energy dissociation spectral structure as well as in the yield. The data clearly indicate temporal effects involving the dissociation paths' dynamics but also molecular alignment. In the present study we have undertaken the effort to analyze our experimental data with support from theoretical calculations. Although we did not fully simulate the actual experimental conditions (molecular alignment, volume integration, and beam propagation effects), we performed *ab initio* time-dependent Schrödinger equation (TDSE) calculations with the  $H_2^+$  assumed in a Frank-Condon initial distribution (following molecular hydrogen ionization). We have found a general agreement to the measurements, the details of which shed light on the aspects of the dynamics of the dissociation paths.

In the following Sec. II, we present the experimental approach followed in the measurements including the critical pulse duration determination. Next, in Sec. III we present the theoretical formulation including the underlying physical aspects of the dissociation mechanisms in a Floquet picture. Finally, in Sec. IV we present our experimental findings on the dissociation mechanisms due to the pulse duration effects accompanied by the details of the theoretical results.

**II. EXPERIMENTAL APPROACH**

The core of the light source of the CPPL-TEI of Crete facility is a Femtolasers Produktions GmbH 10-pass Ti:sapphire 1-kHz repetition rate laser amplifier that is designed to deliver

ultrashort pulses with durations of 35 fs or few-cycle pulses with durations of 7 fs having the option of carrier envelope phase (CEP) stabilization. For the current measurements CEP stabilization was not a requisite. In the latter case, the 35-fs pulse are loosely focused in a 1-m hollow fiber filled with Ne at a typical pressure of 2 atm. The resulting bandwidth broadened pulses are then guided into a set of four pairs of specially designed negatively chirped multilayer mirrors with the ability to compress the pulse to sub-7-fs duration. A pair of thin wedged plates at the exit of the compressor optionally allows for finely compensating for the negative chirp and thus achieving the shortest pulse supported by the bandwidth (Fourier-transform limited or FTL). The pulse duration is accurately measured by a second-order shot-to-shot autocorrelator designed to measure pulses as short as 5 fs.

The experimental setup is illustrated in Fig. 1. The 7-fs laser beam is guided into the interaction vacuum chamber entering through a 1-mm-thick fused silica (FS) window. A 250- $\mu\text{m}$ -thick half wave plate placed at the entry of the hollow fiber tube and a pair of Si plates at Brewster angle located at the chamber area are utilized for controlling the laser beam intensity. The duration of the pulses is measured by the second-order shot-to-shot autocorrelator located at the vicinity of the chamber in order to take into account the broadening effects due to the propagation in the air and the optical components including the entry FS glass. The beam is focused on axis by a 25-cm focal length broadband spherical mirror. The chamber was pumped down via a 250-l/s turbomolecular pump at a base pressure of  $3 \times 10^{-7}$  mbar and flooded with  $\text{H}_2$  up to a pressure of  $2 \times 10^{-6}$  mbar. The spectrometer was designed to provide a constant low extraction field (10 V/cm) suitable for detecting low-energy fragments, much like the one used in standard COLTRIMS devices [28]. It consists of 21 thin

circular plates of 70 mm outer diameter and 35 mm inner diameter, equally spaced by 10 mm. The plates are electrically connected consecutively with 100 k $\Omega$  resistors having a total voltage difference of 100 V terminated at a grounded fine mesh of 90% transmission. The thus formed constant low field serves as a time-of-flight (TOF) spectrometer capable of resolving backward-forward low-energy ionic fragments. The interaction area is defined by the focal volume of the laser beam and the resulting ions are detected by a multichannel plate detector coupled to a 1-GHz, 5-Gs oscilloscope triggered by a fast photodiode signal.

The ionic yields were collected as a function of the laser pulse duration. This was achieved by introducing  $\text{MgF}_2$  plates along the laser beam of variable thickness covering a range between 1 and 8 mm. For each thickness the laser intensity was adjusted appropriately, as it will be justified later on in the paper, utilizing the set of half wave plate and Brewster plates. At the same time the second-order AC trace of the pulse was recorded as well in order to accurately determine the duration of the laser pulse. The exploitation of the low-field TOF spectrometer in the measurements was decided upon for the necessity for increased efficiency in the detection of slow ions. However, the ionic yield of this low-field TOF spectrometer is sensitive to the geometry of the active target area, as opposed to TOF spectrometers with small holes in the extraction plates. Thus, special care was taken to maintain identical experimental conditions throughout the measurements.

Typical second-order interferometric AC traces corresponding to the duration of the laser pulses are presented in Fig. 2. The pulses were delivered at a small negative chirp at the entry of the chamber, as it was checked by measuring their duration without the FS plate compensator. The positive chirp introduced by the 1-mm-thick FS plate was adequate to reach the optimum conditions of almost FTL pulses having durations of 7 fs. The accurate extraction of the duration of the pulse from the AC trace was performed as follows. Electric-field pulses having Gaussian temporal profile and accounting for the chirp

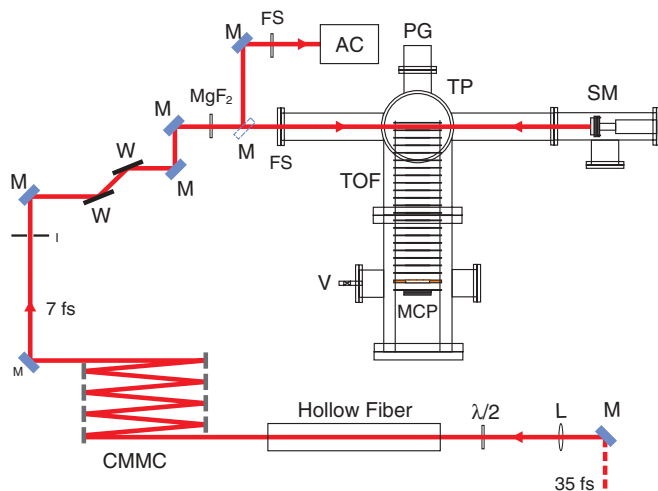


FIG. 1. (Color online) General overview of the experimental setup. M: broadband mirrors, SM: broadband spherical mirror, L: 1-m focal length lens, CMMC: Chirped multilayer mirrors compressor, AC: second-order shot-to-shot autocorrelator, I: iris, W: Brewster plates,  $\lambda/2$ : half wave plate, FS: 1-mm fused silica window, V: leak valve, PG: pressure gauge, TP: turbomolecular pump, TOF: time-of-flight spectrometer, MCP: multichannel plates detector.

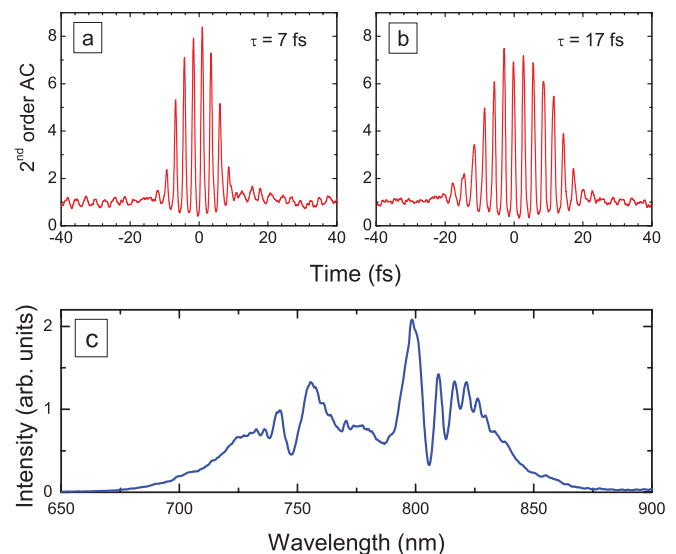


FIG. 2. (Color online) Measurements of second-order interferometric AC traces of (a) 7-fs FTL (b) and 17-fs chirped pulses. (c) Indicative spectra supporting 7-fs laser pulses.

through the second-order dispersion parameter  $D_2$  were used as the seed for generating second-order interferometric AC traces. These pulses are described by

$$E(t, D_2) = E_1(t, D_2) \exp \{ i [\omega_0 t - \phi(t, D_2)] \}, \quad (1)$$

where

$$E_1(t, D_2) = \frac{E_0 \sigma_I}{\sqrt[4]{\sigma_I^4 + D_2^2}} \exp \left[ -\frac{t^2 \sigma_I^2}{2(\sigma_I^4 + D_2^2)} \right]$$

and

$$\phi(t, D_2) = -\frac{D_2}{2(\sigma_I^4 + D_2^2)} t^2 + \frac{1}{2} \arctan \left( \frac{D_2}{\sigma_I^2} \right).$$

The standard deviation  $\sigma_I$  of the Gaussian corresponds to a full width at half maximum (FWHM) of 7 fs, i.e., to an FTL pulse at the interaction area as determined experimentally. The second-order dispersion  $D_2$ , introduced by the MgF<sub>2</sub> plates, was reserved as the fitting parameter. Its value was determined by the comparison of the generated AC traces to the measured one. Once the value of  $D_2$  was determined, the pulse duration was obtained by the FWHM of the intensity of the corresponding seed pulse. A typical broadband laser spectrum adequate for supporting 7-fs pulses is shown in Fig. 2(c).

The pulse broadening was also estimated by taking into account the value of the second-order dispersion  $D_2$  at the central wavelength of the laser spectrum and the thickness of the MgF<sub>2</sub> plate. The agreement with the AC simulations was within 5%. The choice of MgF<sub>2</sub> as the material for introducing the chirp was based on its small value of the second-order dispersion. Indeed, MgF<sub>2</sub> has  $D_2 = 22$  fs<sup>2</sup>/mm at 750 nm, as opposed to  $D_2 = 45$  fs<sup>2</sup>/mm at 750 nm for fused silica, for example, allowing for finer steps of chirp addition to the initial FTL pulse, especially for smaller durations in the range 7–29 fs.

### III. THEORETICAL METHODS

In this section we present the theoretical framework and the computational method we have developed in order to study the dynamics of the dissociation channels of H<sub>2</sub><sup>+</sup> under the chirped laser field described by Eq. (1). Furthermore, we also consider an alternative and complementary point of view of the dissociation mechanism to interpret our findings [1]. This consists of the Floquet picture which has been commonly used over the years for both a qualitative and quantitative (depending on the experimental conditions) description of the processes involved. For clarity, the presentation of the theory is in atomic units while in the discussion of the results we use more familiar units which give a direct intuition of the various physical processes involved.

#### A. Computational method

The dynamics of the molecular hydrogen ion is governed by the time-dependent Schrödinger equation (TDSE) with the system's wave function  $\psi(R, \mathbf{r}, t)$  to satisfy

$$i \frac{\partial}{\partial t} \psi(R, \mathbf{r}, t) = [\hat{H}_0 + \hat{D}(\mathbf{r}, t)] \psi(R, \mathbf{r}, t). \quad (2)$$

In the above,  $R$  denotes the internuclear distance, while by  $\mathbf{r}$  we express the electronic coordinates. The origin of the coordinate system is placed in the middle of the internuclear axis. The quantity  $D(\mathbf{r}, t)$  representing the field-molecule interaction operator, in the dipole approximation, is expressed as  $\hat{D}(\mathbf{r}, t) = -\mathcal{E}(t) \mathbf{e}_z \cdot \mathbf{r}$ , with the field assumed linearly polarized along the  $z$  axis and  $\mathbf{e}_z$  denoting the unit field's polarization vector.

To proceed further, we adopt the Born-Oppenheimer (BO) approximation and write the total wave function as

$$\psi(R, \mathbf{r}, t) = \sum_{q=g,u} \frac{1}{R} F_q(R, t) \Phi_q(R, \mathbf{r}), \quad (3)$$

which separates the nuclear and electronic coordinates in the terms  $F_q(R, t)$  and  $\Phi_q(R, \mathbf{r})$ , respectively [29]. Within this approximation, the electronic wave function  $\Phi_q(R, \mathbf{r})$  satisfies the following equation:

$$\hat{H}_{el} \Phi_q(R, \mathbf{r}) = E_q(R) \Phi_q(R, \mathbf{r}), \quad q = g, u, \quad (4)$$

with  $H_{el}$  representing the electronic Hamiltonian [29–31]. This Hamiltonian depends on the internuclear distance  $R$  parametrically with  $E_q(R)$  representing the BO potential-energy curve of the  $n$ th electronic state of the molecule. In the above and the following, we have restricted the possible occupied electronic states to be only those of the molecular hydrogen ion  $g \equiv 1s\sigma_g$  (gerade) and  $u \equiv 2p\sigma_u$  (ungerade). This approximation is generally adopted when the hydrogen ion dissociation dynamics is to be studied with pulses having similar characteristics as the one in our experiment. It has been shown that an adequate description of the hydrogen ion dynamics can be obtained while its limitations under various experimental conditions has been studied at a great extent [1,32].

As the focus of the present study is the dissociation process of the molecular hydrogen ion, we do not need to consider the electronic degrees of freedom and we may reduce the dimensionality of the problem. We eliminate the electronic coordinates by projecting the conjugate of  $\Phi_q(R, \mathbf{r})$  from the left of the TDSE and then integrating over the spatial variables of the electron. Doing this, and exploiting the fact that  $\langle \Phi_{q'} | \Phi_q \rangle = \delta_{qq'}$  and  $\langle \Phi_{q'} | H_{el} | \Phi_q \rangle = E_q(R) \delta_{qq'}$ , we end up with the following effective TDSEs for the time-dependent nuclear channel wave functions  $F_q(R, t)$ :

$$i \frac{d}{dt} F_g(R, t) = \hat{H}_g F_g(R, t) - \mathcal{E}(t) \hat{D}_{gu}(R) F_u(R, t), \quad (5a)$$

$$i \frac{d}{dt} F_u(R, t) = \hat{H}_u F_u(R, t) - \mathcal{E}(t) \hat{D}_{ug}(R) F_g(R, t), \quad (5b)$$

where  $\hat{H}_q$  is the effective nuclear Hamiltonian,  $\hat{H}_q(R) = -\nabla_R^2/2\mu + E_q(R)$ ,  $q = g, u$  and  $\mu$  being the system's reduced mass [29]. In the above expression for the effective nuclear Hamiltonian the usual rotational term was ignored (set to zero), assuming that the dissociation process is much faster than any change to the system due to the rotational degrees of freedom. Finally, the effective dipole operator  $D_{qq'}(R)$  is given by the standard expression,  $D_{gu}(R) = \langle \Phi_g | \hat{D} | \Phi_u \rangle = \int d\mathbf{r} \Phi_g^*(R, \mathbf{r}) \mathbf{e}_z \cdot \mathbf{r} \Phi_u(R, \mathbf{r})$ . In order to solve the above derived dissociative TDSEs, we further expand the time-dependent channel nuclear wave function on the eigenstates

of  $\hat{H}_q(R)$ :

$$F_q(R, t) = \sum_n C_{n_q}(t) F_{n_q}(R), \quad q = g, u, \quad (6)$$

with  $F_{n_q}$  satisfying the  $\hat{H}_q F_{n_q}(R) = E_q F_{n_q}(R)$  eigenvalue problem. This expansion implies the so-called *adiabatic Born-Oppenheimer* approximation, which is expected to provide a more accurate description of the dynamics when the pulse becomes shorter or comparable to the induced vibrational characteristic times of the system. This approximation leads to substantial reduction of the computational demands of the numerical problem of propagating the time-dependent dissociative channel wave functions.

Formally, we may label the eigensolutions of the  $H_q$  Hamiltonian with the index  $n_q$ , thus allowing us to represent collectively both the bound ( $E_{n_q} < 0$ ) and continuum ( $E_{n_q} > 0$ ) solutions of  $\hat{H}_q$ . To proceed further, we substitute Eq. (6) in Eqs. (5b) and (5a) and then we project from the left with the conjugate of  $F_{n_q}(R, t)$ . Integration over the nuclear coordinates results in a system of ordinary differential equations for the time-dependent amplitudes  $C_{n_q}$ , as below:

$$i\dot{C}_{n_g}(t) = C_{n_g} E_{n_g} + \mathcal{E}(t) \sum_{n_u} D_{n_g n_u} C_{n_u}(t), \quad (7)$$

$$i\dot{C}_{n_u}(t) = C_{n_u} E_{n_u} + \mathcal{E}(t) \sum_{n_g} D_{n_u n_g} C_{n_g}(t). \quad (8)$$

To arrive at this formulation of the TDSEs we used the orthonormalization properties of the nuclear channel solutions  $\langle F_{n_q} | F_{n_{q'}} \rangle = \delta_{n_q n_{q'}} \delta_{qq'}$ . The dipole transition amplitudes  $D_{n_g n_u}$  are defined as below:

$$D_{n_g n_u} = \int dR F_{n_g}^*(R) D_{gu}(R) F_{n_u}(R). \quad (9)$$

Note that transitions within states of the same symmetry vanish due to parity symmetry reasons. Dipole transitions necessarily end up to transitions between states with different parity. The above equations are the working equations and provided that the eigenvalues  $E_{n_q}, q = g, u$  and the transition amplitudes  $D_{n_g n_u}$  are known (as the only dynamical parameters present in the TDSEs) we may propagate them in time, with the initial conditions [ $C_{n_q}(0) = \delta_{n_q 1_g}$ ] and obtain the coefficients  $C_{n_q}(t)$  after the end of the pulse. The value of  $P_{n_q} = |C_{n_q}(t \rightarrow \infty)|^2$  provides the probability to detect the system at time  $t$  (after the pulse has vanished) in the nuclear state  $\Phi_{n_q}$ , determined from the electronic potential  $E_q(R)$ . Finally, the kinetic-energy release (KER) spectrum is obtained as  $S(E) = \sum_{q=g,u} S_q(E)$ , where the partial KERs are obtained as

$$S_q(E > 0) = \sum_{E_{n_q} < E < E_{n_{q+1}}} \rho_{n_q}(E) |C_{n_q}(t \rightarrow \infty)|^2, \quad (10)$$

where  $\rho_{n_q}(E)$  is the appropriate density for the continuum dissociation states [33].

To complete the calculation procedure we need to solve the eigenvalue equations for the electronic potentials  $E_g(R)$  and  $E_u(R)$  we follow an approach where the system is placed in a spherical box which effectively discretizes the continuum spectrum, a method that has been applied with success in both complex atomic and molecular systems [29,34–38]. The

nuclear eigenstates are then expressed in terms of known B-splines polynomials which, after imposing zero boundary condition at both edges of the spherical box, transforms the problem to a matrix generalized eigenvalue problem, which, by now, can be solved using standard numerical approaches. The reader can find the details of this approach in a number of our earlier works while for further details on the particular implementation one should refer to Ref. [29]. The electronic potential for the  $u$  and  $g$  states were represented by a Morse potential, while the effective dipole operator  $D_{gu}(R)$  was taken from [32,39]. The number of the B-splines basis was 800 and their order was 9. We choose a box radius of 50 a.u. to ensure that there is an insignificant probability for the dissociation fragments to reach the boundary of our box, within the pulse duration. The adoption of a large box allowed us to avoid the inclusion of absorbing potential in the propagation of the wave function later on. Our solutions resulted in eigenenergy values which are in excellent agreement with known experimental values. We have also compared our values with those presented in Ref. [29] and ensured agreement to six digits.

## B. Dissociation mechanism based on the Floquet approximation

Despite the numerical treatment of the problem after solving the corresponding dissociative TDSEs, it would be both instructive and convenient to view the problem in the perspective of the Floquet picture depicted in Fig. 3. Within the Floquet approximation, the system is described by the field-dressed states which are the product of the molecular states  $|q\rangle$  and the photon-number states  $|N\rangle$ , denoted as  $|q, N\rangle$ ,  $q = u, g$  in our case. In general, the Floquet representation is valid when the field contains a number of cycles, and as such we shall mostly use it to discuss the cases with the longest pulses in the present experiment. Note that the relevant times in the experiment are the laser pulse duration ranging 7–55 fs and the  $\text{H}_2^+$  ground state vibrational period  $\simeq 14$  fs. Assuming that initially we have  $N = 0$ , in the dressed state picture, the absorption of one photon leads to the state  $|u, -1\omega\rangle$

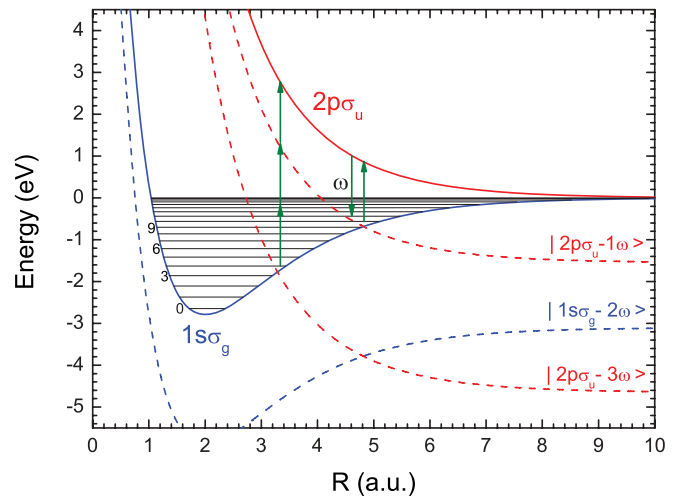


FIG. 3. (Color online)  $1s_g$  and  $2p\sigma_u$  potential-energy curves of  $\text{H}_2^+$  along with their dressed diabatic companions in the Floquet picture. The vibrational states of the bound  $1s_g$  state along with the BS ( $1\omega$ ) and ATD ( $2\omega$ ) dissociation channels are depicted as well.

which becomes degenerate with the initial state  $|g, 0\omega\rangle$ . Due to this field-induced degeneracy their potential energies have the tendency to cross each other (diabatic crossing). A transition between the two states is then possible, which may lead the molecular dissociation to resonate exactly at this cross point as shown in Fig. 3. The kinetic-energy release spectrum resulting from the above transition, assuming it is a one-photon crossing, is simply estimated by taking the energy difference between the diabatic  $1\omega$  crossing and the asymptotic limit of the  $|u, -1\omega\rangle$  state. The same reasoning applies to higher-order crossings. Moreover, by taking into account the coupling between the diabatic dressed states one results in avoided crossings at the points of diabatic crossings, the gap of which depends on the laser intensity and the order of the crossing. The thus obtained adiabatic dressed states lay the foundation for understanding the dissociation paths. The picture for our particular experiment is as follows.

Initially, the molecule sees the trailing edge of the pulse where the ionization takes place primarily through a multiphoton process. The ionization of the neutral hydrogen leaves the  $\text{H}_2^+$  ionic molecule in a Frank-Condon population distribution for the vibrational states. Even though this assumption may not be entirely correct, depending on the experimental conditions [40–42], it does not distort decisively the dynamics of the dissociation mechanisms. Subsequently, the ionized molecule of  $\text{H}_2^+$  is found in stronger parts of the laser field that deforms the molecular potential initiating the dissociation processes. In the Floquet picture we may say that diabatic potentials become coupled at the crossings leading to the adiabatic avoided crossings which become larger as the electric-field strength increases. Then, the population of the vibrational states that lie below the diabatic crossings of the  $|g, 0\omega\rangle$  and  $|u, -1\omega\rangle$  curves will either dissociate or tunnel through the barrier. The process is commonly called bond softening and relates to the one-photon process. The same picture is repeated at higher field values for the diabatic crossings of the  $|g, 0\omega\rangle$  and  $|u, -3\omega\rangle$  and is known as above threshold dissociation. It involves a three-photon absorption and one-photon emission as the molecular wave packet passes through the one-photon crossing ( $\simeq 4.8$  a.u. internuclear distance) where the  $|g, 0\omega\rangle$  and  $|u, -1\omega\rangle$  states are strongly coupled via the still intense laser field. It is important to mention that both pictures, i.e., Floquet and photon absorption and/or emission, are equivalent. In this spirit the BS and ATD processes are referred to as  $1\omega$  and  $2\omega$  paths, respectively.

Having considered the experimental conditions and the theoretical background of the present work we turn now to the presentation of our findings and the associated discussion.

#### IV. RESULTS AND DISCUSSION

The majority of the studies on the laser induced  $\text{H}_2^+$  dissociation utilized FTL pulses with durations between 30 and 100 fs. However, it is evident that pulses having identical bandwidth but different temporal structure may result in different spectra mapping the separation of the colors inside the laser pulse as has been shown in the literature [26]. In order to expose such effects the pulse duration has to be broadened so that both the colors of the pulse are well separated in time and the physical process is completed at times shorter than

the final pulse duration. Aside from this, chirp may play an important role through the control of the laser pulse duration in cases where the two aforementioned conditions are not met. Then, processes sensitive to the duration of the pulse, such as molecular alignment or dissociation, can be traced by simply varying, through the positive chirp, the duration of the laser pulse. In this work, this method is followed in order to monitor the dynamics of the dissociation paths of BS and ATD in  $\text{H}_2^+$  dissociation when interacting with few-cycle laser pulses.

In such studies, comparison of the data at equal laser peak intensities might not be insightful since the evolution of a nonlinear process depends both on the peak intensity as well as on the pulse duration. For example, for long laser pulses, i.e., pulses that last many laser periods, molecular alignment may well be established during the interaction of the molecule with the pulse while in the case of short laser pulses, having duration of a few laser periods, the process is not completed during the interaction leading to different outcomes. In these cases, it is preferable to compare data against peaks arising from simpler processes such as single ionization. Indeed, such an approach had been introduced earlier in the literature [3]. It is a universal way of tracking secondary processes based on the simpler and well-understood multiphoton ionization, assuring in addition the experimental reproducibility free of questionable parameter determination such as the accurate value of the laser peak intensity [43].

Thus, the presented data on  $\text{H}_2^+$  dissociation were obtained by carefully adjusting the laser intensity, via the set of half wave plate and Brewster plates, in order to correspond to equal yields of molecular hydrogen single ionization ( $\text{H}_2^+$  signal). The situation is depicted in the typical TOF spectra corresponding to 7-fs FTL pulses and 45-fs chirped pulses presented in Fig. 4. Following this experimental approach

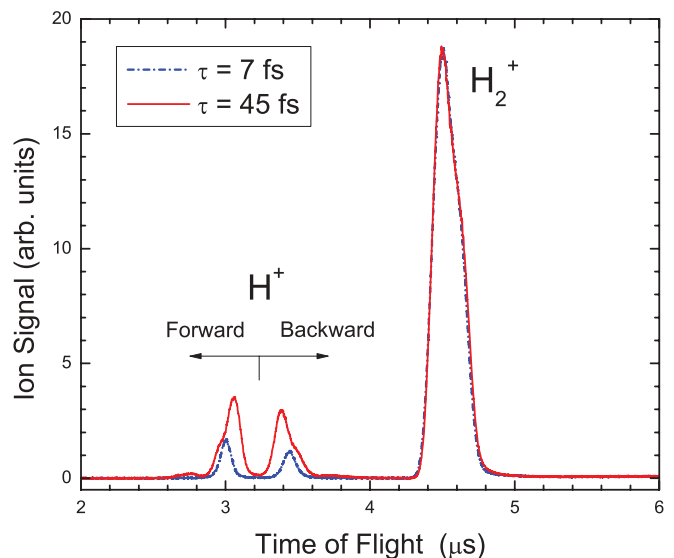


FIG. 4. (Color online) Typical spectra of  $\text{H}_2$  ionization and  $\text{H}_2^+$  dissociation under strong-field laser pulses. The dashed (blue) line corresponds to 7-fs FTL pulses recorded at a peak intensity of  $1.0 \times 10^{14}$  W/cm<sup>2</sup>. The solid (red) line corresponds to 45-fs chirped pulses broadened from the 7-fs pulses recorded at a peak intensity of  $0.5 \times 10^{14}$  W/cm<sup>2</sup>. Note that both  $\text{H}^+$  dissociation spectra were recorded for equal  $\text{H}_2^+$  signals.

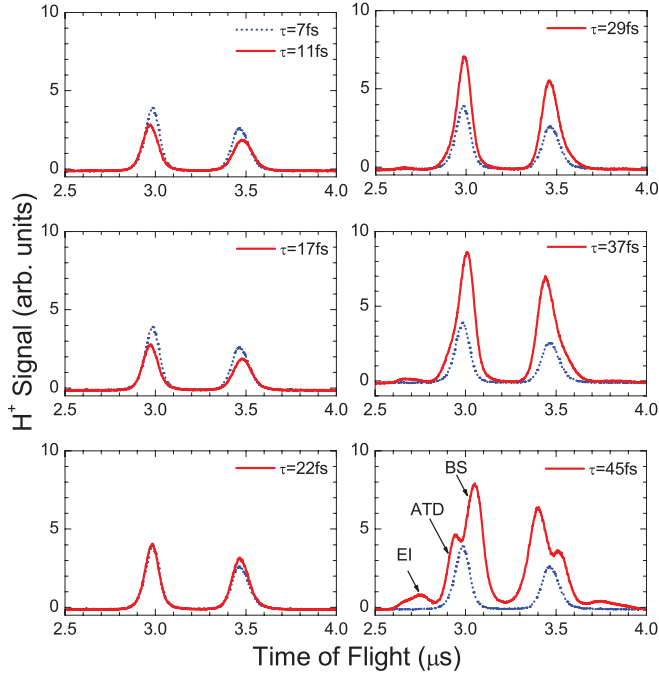


FIG. 5. (Color online) Comparative  $\text{H}_2^+$  dissociation yields at different laser pulse durations. All data correspond to equal  $\text{H}_2^+$  ionization yield. The dashed (blue) line corresponds to 7-fs pulses and the solid (red) line to all the other pulse durations.

the dissociation signals of  $\text{H}_2^+$  were recorded for laser pulse durations covering the range 7–55 fs in fine steps at four sets of laser peak intensities between  $0.5$  and  $1.0 \times 10^{14} \text{ W/cm}^2$ .

In Fig. 5 a typical set of the aforementioned data is presented. The comparative presentation shows clearly the dynamical change in both the magnitude of the yields as well as the structure of the spectrum. Initially, for 7-fs pulses, the yields referred to as BS and ATD are recorded in a single peak while EI remains undetected at these intensities. This fact is not due to the spectrometer resolution but is rather an intrinsic characteristic of the processes at such short pulses, as also recorded by other groups [13], and will be clarified later on in the paper. BS and ATD yields then decrease substantially from their value at 7 fs to recover for duration close to 22 fs. When the pulse duration reaches 29 fs the yield is almost doubled compared to the 7-fs case. For pulses longer than 40 fs the separation of the BS and ATD peaks appears along with the appearance of the EI peak. It is worth noticing that the estimated peak intensities drop rapidly from the value of  $1.0 \times 10^{14} \text{ W/cm}^2$  at 7 fs to  $0.5 \times 10^{14} \text{ W/cm}^2$  at 17 fs to remain essentially unchanged up to duration of 55 fs. As it was mentioned earlier, even though we chose to perform this study at equal  $\text{H}_2^+$  yields for all laser pulse durations it turned out that for durations higher than 17 fs the peak intensity remained essentially constant to the value of  $5 \times 10^{13} \text{ W/cm}^2$  to an experimentally determined error of  $\sim 10\%$ . This counterintuitive observation is the first of our findings resulting from the incremental systematic variation of the pulse duration depicting the strong dependence of the single ionization on the peak intensity as compared to the weaker dependence on the pulse duration, at least for the durations used in this study.

### A. Alignment effects

In Fig. 5 the reduction of the BS and ATD yields for durations between 7 and 22 fs is observed. This should be primarily attributed to the decrease of the laser peak intensity. Based on the requirement that the  $\text{H}_2^+$  yields are equal for all cases, the reduction in the  $\text{H}_2^+$  yield due to the reduction of the peak intensity is inevitably compensated by the increase in the pulse duration. However, this behavior is not followed by the  $\text{H}^+$  yield, possibly due to the higher nonlinear character of the dissociation processes as compared to the multiphoton single ionization. The situation is considerably altered for durations between 22 and 55 fs. The fact that the peak intensities remain essentially unchanged in this temporal range implies that the variations in the dissociation yields should be directly connected to the durations of the pulses. Thus, dynamic molecular alignment effects, i.e., effects due to the induced molecular alignment imposed by the laser field, should be considered. Indeed, dynamic molecular alignment enhances dissociation processes such as BS and ATD that are evolving along the molecular axis. On the other hand, dissociation at shorter pulses is concluded primarily due to geometrical alignment, i.e., dissociation by molecules statistically fixed along the polarization axis of the laser pulse during their interaction. In more detail, molecules whose axis is at an angle  $\theta$  with the polarization axis will experience a smaller electric field according to  $E = E_0 \cos \theta$  and therefore a smaller laser peak intensity that might not be adequate to initiate dissociation processes. As a result, only the fraction of the molecules that is initially geometrically aligned and during the pulse duration dynamically aligned will dissociate via the BS and ATD processes.

We may infer from the literature that maximum dynamic alignment of molecular hydrogen occurs at  $\simeq 20$  fs [44]. As a consequence, the dissociation yield is expected to be substantially enhanced around this temporal duration. Indeed, our data support this finding as the yield increases substantially between 17- and 22-fs pulse durations where the dynamic alignment is expected to be significant although not yet peaked. The yield is increased at higher rates between 22- and 29-fs pulse durations implying that the alignment process is peaking. In order to quantify this argument we plot in Fig. 6 the ratio of the yields between the BS and ATD ( $\text{H} + \text{H}^+$ ) dissociation channels and the  $\text{H}_2^+$  ionization for all pulse durations and all the sets of laser peak intensities. The gradual appearance of the molecular alignment, qualitatively evident in Fig. 5, is quantitatively established. The rapid increase of the dissociation yield between durations of 22 and 29 fs implies that the major contribution of the dynamical alignment takes place at this time interval. The yield keeps increasing for longer durations, although not as rapidly as in the later time interval as a result of the depletion of the population of the nonaligned  $\text{H}_2$  molecules. Moreover, after  $\simeq 50$ -fs duration the ratio decreases as the channel of EI appears. EI is promoted via the BS and ATD channels, therefore its appearance results in a decrease of the yield of the latter two channels.

### B. Pulse duration effects

A summary of all the experimental data and theoretical calculations corresponding to various laser peak intensities

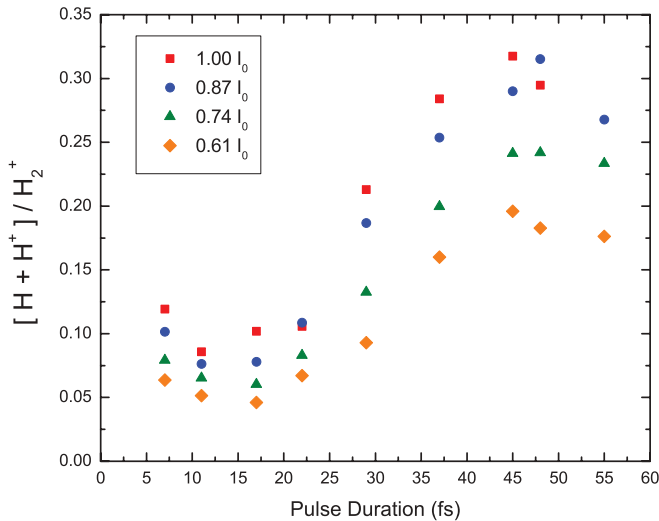


FIG. 6. (Color online) Ratio between the BS and ATD ( $H + H^+$ ) dissociation channels and the  $H_2^+$  ionization.  $I_0$  corresponds to the maximum intensity of  $1.0 \times 10^{14} \text{ W/cm}^2$  for the case of 7 fs.

covering the range 7–55 fs is presented in Fig. 7. The theoretical calculations correspond to a single molecule fixed along the polarization axis of the laser field. Likewise, the intensity difference method was applied to the experimental data in order to reduce the interaction volume effects [45]. Despite this, the comparison cannot be fully quantitative. The experimental yield corresponds to the ionic signal divided by  $\Delta E$ , where  $\Delta E$  is determined by the TOF-KER calibration relation for consistency reasons. The energy calibration was obtained after simulating the spectrometer in the SIMION8.0 ion ray-tracing program. The inferred maximum peak intensity  $I_0$  applies to the case of 7 fs and its value is  $1.0 \times 10^{14} \text{ W/cm}^2$ . From Fig. 7 it is evident that the spectral structure as well as the ionic yield vary considerably at increasing pulse durations. Our calculations are seen to be in agreement with the measurements and reproduce their features at a great extent. Moreover, they have been compared to and found in very good agreement with similar calculations reported in [18,19].

In the following we will try to interpret these changes by using concepts of the Floquet picture, even though the picture is not expected to be valid at short pulse durations lasting only a few cycles of the laser field. The effort is instructive and seeks to set certain limits to the use of the picture in such problems. Initially, we may estimate typical KER values for both dissociation paths assuming diabatic transitions around the dressed potential-curves crossings. For the  $1\omega$  crossing (BS), the transition energy is  $E_9 - E_u \simeq 0.85 \text{ eV}$  while for the  $3\omega$  crossing (ATD) it is  $E_4 - E_g \simeq 1.47 \text{ eV}$ . Since these values refer to diabatic potentials they are valid for relatively low laser intensities (e.g.,  $\sim 1 \times 10^{13}$ ). As described earlier, at these intensities the BS mechanism is effective, thus resulting in the coupling between diabatic potentials at the crossing areas. Therefore the appearance of the gap between them allows for lower vibrational states to dissociate either over the effective barrier or tunnel through it. As a result, the final KERs will be smaller than the ones predicted by the diabatic potentials. For the intensities of this study the above picture describes

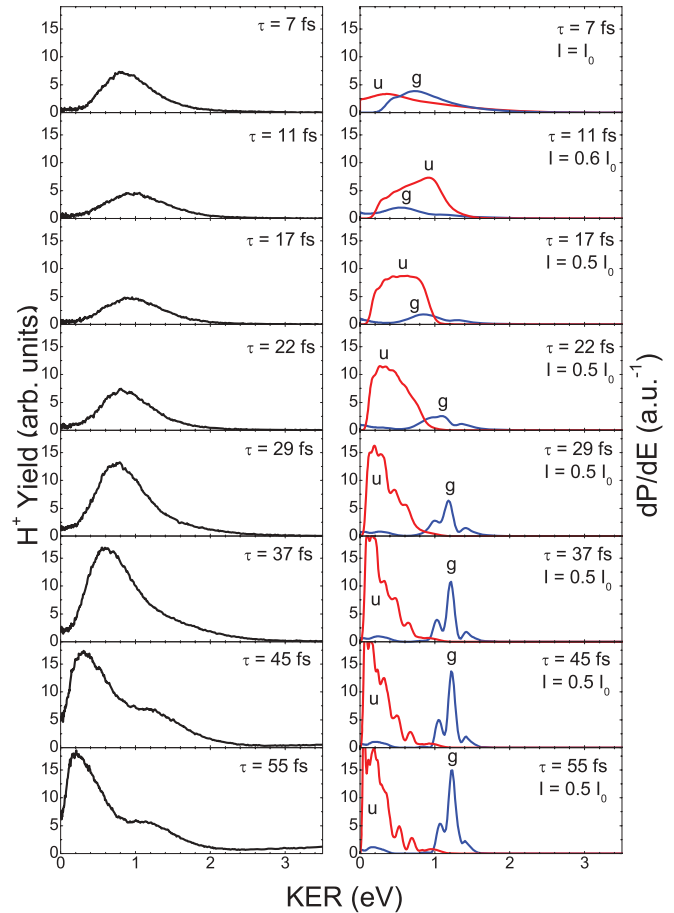


FIG. 7. (Color online) Left: Experimental data on  $H_2^+$  dissociation. The  $H^+$  yield ( $H^+$  signal/ $\Delta E$ ), obtained at equal  $H_2^+$  signals for all cases, is plotted top to bottom at increasing durations of the laser pulse. Right: Theoretical calculations corresponding to the experimental conditions but for one molecule. The contribution of the final dissociation states  $|g\rangle$  or  $|u\rangle$ , corresponding to the ATD and BS paths, are marked in the graph.

accurately the  $1\omega$  crossing as the laser field is quite strong to initiate the BS mechanism. Thus, we would expect that the KER due to  $1\omega$  crossing to be smaller than 0.85 eV, perhaps closer to  $E_5 - E_u \simeq 0.34 \text{ eV}$ . Higher vibrational states than  $v = 5$  are expected to result in higher KERs. However, the peak center should be moved to lower KER values, closer to the  $v = 5$  state, partly accounting for the Frank-Condon vibrational population distribution. For the  $3\omega$  crossing the field is less strong compared to the potentials at the crossing resulting in a less pronounced potential gap. Therefore, the expected KERs will be smaller than estimated but closer to their diabatic values. Finally, we should mention that the above KER estimations will result in broader peaks after taking into account the broad bandwidth of the laser pulse covering an energy range 1.4–1.7 eV.

Keeping in mind the above analysis we follow our experimental data and theoretical calculations at increasing pulse durations as presented in Fig. 7. Certainly, longer durations partially invalidate some of the approximation adopted in the theoretical calculations (Frank-Condon initial distribution for the  $H_2^+$ , adiabatic Born-Oppenheimer approximation) but on

the other hand molecular alignment increases contributing to the justification of the approximations, while the Floquet picture gains, gradually, more credibility. Initially, for the shortest pulse duration of 7 fs, it is clear that both dissociation paths are not spectrally separated but rather highly overlapped around a broad peak at  $\approx 0.8$  eV. This result is in agreement with earlier reports [13,18,19]. The feature is not reproduced by the Floquet predictions, as described earlier, a fact that was expected for such short pulses. The picture remains essentially unchanged for pulses up to 22 fs. At this pulse duration our theoretical calculations show a separation between the two dissociative paths, although it is not evident in the data possibly due to the small signal of the ATD path. However, this feature is experimentally visible for 29-fs pulses where a tail at the initial peak corresponding to the 7-fs case starts to appear. For higher durations the BS and ATD peaks are clearly separate. It is worth mentioning that the low-energy spectra ( $<0.3$  eV) that appear in the  $|g\rangle$  case result from the vibrational states 12–18. Furthermore, the dissociative energies are recorded at the values which are in agreement with the Floquet predictions.

A common feature in both the theoretical calculations and the experimental data is that the BS yield remains largely constant while the ATD yield increases as the pulse duration increases. It should be noted here that the laser peak intensity remains constant for durations higher than 17 fs and only the duration of the pulse varies. This fact is a clear evidence of the role of the laser pulse temporal extent on the yield of a process. ATD signal is initially small at this laser intensity as the field strength is relatively small compared to the potentials value, thus resulting in a small dissociation rate. However, as the duration of the pulse increases the dissociation rate is enhanced not due to the increase of the field strength but rather due to the temporal broadening.

In order to further investigate the problem, we have studied theoretically the contribution of each vibrational state to both dissociation paths. A comparative study corresponding to laser peak intensity of  $5 \times 10^{13}$  W/cm<sup>2</sup> is presented in Fig. 8. The 7-fs case is also presented at this value of peak intensity for consistency reasons. Starting from the 45-fs case and the ATD path, we see that the main vibrational states that contribute to this path are the  $v = 3, 4$  and  $v = 5$ . This is in accordance to the Floquet picture since these states are in the neighborhood of the  $3\omega$  crossing. Higher vibrational levels do not seem to contribute substantially. The main reason is that the higher levels are closer to the  $1\omega$  crossing and preferably contribute to the BS path rather than the ATD, at least for the peak intensities in this study.

The picture is more complicated for the BS path. A central contribution seems to come from the  $v = 5$  vibrational state. The corresponding energy for the  $1\omega$  transition based on the diabatic potentials is  $E_5 - E_u \approx 0.12$  eV which implies that the state lies close to the top of the effective diabatic barrier. Lower vibrational states do not seem to contribute primarily due to their higher contribution to the ATD path as they are closer to the  $3\omega$  crossing. Higher vibrational states contribute substantially covering an energy range between 0 and 1 eV. Vibrational states  $v \geq 9$  result in higher KER than the  $v = 5$  as expected. However, states with  $v = 6-8$  result in lower KER with structure in their spectrum. The interpretation of

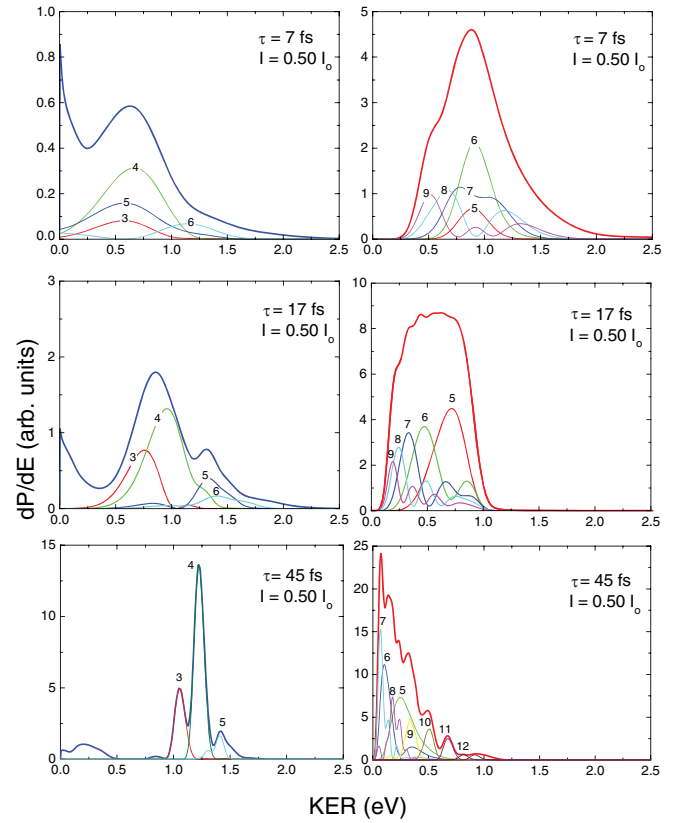


FIG. 8. (Color online) Theoretical calculations. Contribution of the main vibrational states to the dissociation paths for equal laser peak intensities and variable pulse durations. The numbers marked on the curves correspond to the levels of the vibrational states. The thick line corresponds to the sum of all vibrational states. Left: ATD path. Right: BS path.

this behavior lies in the fact that they are located between the  $1\omega$  and  $3\omega$  crossings.

In the case of 7 fs the situation is quite different. In the ATD case the vibrational states that contribute are all the states higher than the level  $v = 3$  with major contributions from states  $v = 3-5$ . The energy distribution for each transition is wider than the 45-fs case and actually wider than the bandwidth of the pulse. In the BS case a clear contribution comes from the  $v = 6$  state. However, the contributions of the higher levels show a structured energy spectrum that is peaking at both lower and higher energies around the value of the  $v = 6$  transition. This behavior is hard to model within the Floquet picture. The very steep change of the intensity of the ultrashort pulse seems to dominate the dissociation processes. Essentially, they are concluded within one or two periods of the pulse while the intensity varies substantially by more than a factor of 2 during the processes. As a result BS and ATD may well be realized at a broad range of intensities resulting both in wide energy distributions as well as in structured peaks. After increasing the pulse duration to 17 fs the situation is still unclear, however, the main features of the Floquet picture have begun to emerge. That is, the ATD path is spectrally separating from the BS path while the vibrational level contributions of the BS path are less structured.

## V. CONCLUSIONS

We have exploited few-cycle laser pulses to systematically investigate the dynamics of the fundamental dissociation processes of BS and ATD in the  $\text{H}_2^+$  dissociation as a function of the laser pulse duration. The two dissociation paths were monitored through their energy dissociation spectra as a function of the pulse duration which was accurately varied via an imposed positive chirp. Our results show unambiguous distinctive characteristics both in the KER spectra for the two paths as well as in the magnitude of their yield for increasing pulses durations. In our findings it is evident that the corresponding KERs of the BS and ATD dissociation paths are seen to overlap for durations shorter than  $\simeq 30$  fs while they are clearly separated for longer pulse durations. In addition, the ATD yield is seen to increase as the pulse duration broadens as opposed to BS which remains largely constant. Strong molecular alignment for durations longer than 20 fs is also evident. These characteristics are directly connected to the underlying physics of dissociation paths governed primarily by the laser pulse temporal extent. In our work we trace their temporal emergence in a systematic and detailed manner. Towards the interpretation of our findings we

benefited by theoretical results of *ab initio* TDSE calculations that were found to be in agreement with the measurements at a great extent. The calculations exposed the contribution of each vibrational state of the  $\text{H}_2^+$  ion to the dissociation paths and the involved dynamics and thus directly connect it to the role of the temporal extent of the laser pulse. The Floquet picture was also adopted for a more convenient understanding of the processes but also to examine the limits of its applicability.

## ACKNOWLEDGMENTS

This research has been co-financed by the European Union (European Social Fund, ESF) and Greek national funds through the Operational Program “Education and Lifelong Learning” of the National Strategic Reference Framework (NSRF) – Research Funding Program: THALIS: Investing in knowledge society through the European Social Fund. L.A.A.N. acknowledges discussions with Dr. Lars Madsen at the initial phase of this work. E.P.B. acknowledges discussions with Professor C. Kosmidis throughout this work.

- 
- [1] J. H. Posthumus, *Rep. Prog. Phys.* **67**, 623 (2010).
  - [2] P. H. Bucksbaum, A. Zavriyev, H. G. Muller, and D. W. Schumacher, *Phys. Rev. Lett.* **64**, 1883 (1990).
  - [3] L. J. Frasinski, J. H. Posthumus, J. Plumridge, K. Codling, P. F. Taday, and A. J. Langley, *Phys. Rev. Lett.* **83**, 3625 (1999).
  - [4] A. Zavriyev, P. H. Bucksbaum, H. G. Muller, and D. W. Schumacher, *Phys. Rev. A* **42**, 5500 (1990).
  - [5] K. Codling, L. J. Frasinski, and P. A. Hatherly, *J. Phys. B* **22**, L321 (1989).
  - [6] T. Zuo and A. D. Bandrauk, *Phys. Rev. A* **52**, R2511 (1995).
  - [7] P. B. Corkum, *Phys. Rev. Lett.* **71**, 1994 (1993).
  - [8] A. S. Alnaser, T. Osipov, E. P. Benis, A. Wech, B. Shan, C. L. Cocke, X. M. Tong, and C. D. Lin, *Phys. Rev. Lett.* **91**, 163002 (2003).
  - [9] A. S. Alnaser, B. Ulrich, X. M. Tong, I. V. Litvinyuk, C. M. Maharjan, P. Ranitovic, T. Osipov, R. Ali, S. Ghimire, Z. Chang *et al.*, *Phys. Rev. A* **72**, 030702 (2005).
  - [10] H. Niikura, D. M. Villeneuve, and P. B. Corkum, *Phys. Rev. A* **73**, 021402 (2006).
  - [11] T. Ergler, A. Rudenko, B. Feuerstein, K. Zrost, C. D. Schröter, R. Moshhammer, and J. Ullrich, *Phys. Rev. Lett.* **97**, 193001 (2006).
  - [12] V. Roudnev, B. D. Esry, and I. Ben-Itzhak, *Phys. Rev. Lett.* **93**, 163601 (2004).
  - [13] M. F. Kling, C. Siedschlag, A. J. Verhoef, J. I. Khan, M. Schultze, T. Uphues, Y. Ni, M. Uiberacker, M. Drescher, F. Krausz *et al.*, *Science* **312**, 246 (2006).
  - [14] M. Kremer, B. Fischer, B. Feuerstein, V. L. B. de Jesus, V. Sharma, C. Hofrichter, A. Rudenko, U. Thumm, C. D. Schröter, R. Moshhammer *et al.*, *Phys. Rev. Lett.* **103**, 213003 (2009).
  - [15] G. N. Gibson, M. Li, C. Guo, and J. Neira, *Phys. Rev. Lett.* **79**, 2022 (1997).
  - [16] F. Légaré, I. V. Litvinyuk, P. W. Dooley, F. Quéré, A. D. Bandrauk, D. M. Villeneuve, and P. B. Corkum, *Phys. Rev. Lett.* **91**, 093002 (2003).
  - [17] A. Staudte, D. Pavičić, S. Chelkowski, D. Zeidler, M. Meckel, H. Niikura, M. Schöffler, S. Schössler, B. Ulrich, P. P. Rajeev *et al.*, *Phys. Rev. Lett.* **98**, 073003 (2007).
  - [18] J. McKenna, A. M. Sayler, F. Anis, B. Gaire, N. G. Johnson, E. Parke, J. J. Hua, H. Mashiko, C. M. Nakamura, E. Moon *et al.*, *Phys. Rev. Lett.* **100**, 133001 (2008).
  - [19] J. McKenna, F. Anis, A. M. Sayler, B. Gaire, N. G. Johnson, E. Parke, K. D. Carnes, B. D. Esry, and I. Ben-Itzhak, *Phys. Rev. A* **85**, 023405 (2012).
  - [20] M. R. Thompson, M. K. Thomas, P. F. Taday, J. H. Posthumus, A. J. Langley, L. J. Frasinski, and K. Codling, *J. Phys. B* **30**, 5755 (1997).
  - [21] I. V. Litvinyuk, A. S. Alnaser, D. Comtois, D. Ray, A. T. Hasan, J.-C. Kieffer, and D. M. Villeneuve, *New J. Phys.* **10**, 083011 (2008).
  - [22] F. He, C. Ruiz, and A. Becker, *Phys. Rev. Lett.* **99**, 083002 (2007).
  - [23] D. Ray, F. He, S. De, W. Cao, H. Mashiko, P. Ranitovic, K. P. Singh, I. Znakovskaya, U. Thumm, G. G. Paulus *et al.*, *Phys. Rev. Lett.* **103**, 223201 (2009).
  - [24] F. Kelkensberg, C. Lefebvre, W. Siu, O. Ghafur, T. T. Nguyen-Dang, O. Atabek, A. Keller, V. Serov, P. Johnsson, M. Swoboda *et al.*, *Phys. Rev. Lett.* **103**, 123005 (2009).
  - [25] B. Moser and G. N. Gibson, *Phys. Rev. A* **80**, 041402 (2009).
  - [26] V. S. Prabhudesai, U. Lev, A. Natan, B. D. Bruner, A. Diner, O. Heber, D. Strasser, D. Schwalm, I. Ben-Itzhak, J. J. Hua *et al.*, *Phys. Rev. A* **81**, 023401 (2010).
  - [27] P. Q. Wang, A. M. Sayler, K. D. Carnes, J. F. Xia, M. A. Smith, B. D. Esry, and I. Ben-Itzhak, *Phys. Rev. A* **74**, 043411 (2006).
  - [28] R. Dörner, V. Mergel, O. Jagutzki, L. Spielberger, J. Ullrich, R. Moshhammer, and H. Schmidt-Böcking, *Phys. Rep.* **330**, 95 (2000).
  - [29] M. Fernando, *J. Phys. B* **32**, R197 (1999).

- [30] H. A. Leth, L. B. Madsen, and K. Mølmer, *Phys. Rev. Lett.* **103**, 183601 (2009).
- [31] H. A. Leth, L. B. Madsen, and K. Mølmer, *Phys. Rev. A* **81**, 053409 (2010).
- [32] Liang-You Peng, I. D. Williams, and J. F. McCann, *J. Phys. B* **38**, 1727 (2005).
- [33] S. Barmaki, S. Laulan, H. Bachau, M. Ghalim, and F. Martin, *J. Phys. B* **36**, 817 (2003).
- [34] M. Venuti, P. Decleva, and A. Lisini, *J. Phys. B* **29**, 5315 (1996).
- [35] L. A. A. Nikolopoulos and P. Lambropoulos, *Phys. Rev. A* **56**, 3106 (1997).
- [36] H. Bachau, E. Cormier, P. Decleva, J. E. Hansen, and F. Martin, *Rev. Mod. Phys.* **64**, 1815 (2001).
- [37] L. A. A. Nikolopoulos, *Comput. Phys. Commun.* **150**, 140 (2003).
- [38] L. A. A. Nikolopoulos, *Phys. Rev. A* **73**, 043408 (2006).
- [39] F. V. Bunkin and I. I. Tugov, *Phys. Rev. A* **8**, 601 (1973).
- [40] X. Urbain, B. Fabre, V. M. Andrianarijaona, J. Jureta, J. H. Posthumus, A. Saenz, E. Baldit, and C. Cornaggia, *Phys. Rev. Lett.* **92**, 163004 (2004).
- [41] T. K. Kjeldsen and L. B. Madsen, *Phys. Rev. Lett.* **95**, 073004 (2005).
- [42] M. Awasthi and A. Saenz, *J. Phys. B* **39**, S389 (2006).
- [43] A. S. Alnaser, X. M. Tong, T. Osipov, S. Voss, C. M. Maharjan, B. Shan, Z. Chang, and C. L. Cocke, *Phys. Rev. A* **70**, 023413 (2004).
- [44] I. A. Bocharova, H. Mashiko, M. Magrakvelidze, D. Ray, P. Ranitovic, C. L. Cocke, and I. V. Litvinyuk, *Phys. Rev. A* **77**, 053407 (2008).
- [45] P. Wang, A. M. Saylor, K. D. Carnes, B. D. Esry, and I. Ben-Itzhak, *Opt. Lett.* **30**, 664 (2005).